

# Imaging shallow objects and heterogeneities with scattered guided waves

G rard C. Herman <sup>\*</sup>      Paul A. Milligan <sup>†</sup>      Robert Huggins <sup>‡</sup>

James W. Rector III <sup>§</sup>

February 10, 1998

## Abstract

Current surface seismic reflection techniques based on the common-mid-point (CMP) reflection stacking method can not be readily used to image small objects in the first few meters of the weathered layer. We discuss a seismic imaging method which uses the first-arrival (guided) wave, scattered by shallow heterogeneities and converted into scattered Rayleigh waves, to detect such objects. These guided waves and Rayleigh waves are dominant in the shallow weathered layer, and are thus suitable for shallow object imaging. We applied this method to a field data set and found that we could certainly image meter-size objects up to about 3 m off to the side of a survey line consisting of vertical geophones. There are indications that crossline horizontal geophone data could be used to identify shallow objects up to 10 m off line in the same region.

Running title: **Imaging shallow objects**

---

<sup>\*</sup>Centre for Technical Geoscience, Delft University of Technology, Mekelweg 4, 2628 CD Delft, The Netherlands.

<sup>†</sup>Engineering Geoscience, Building 90, Room 2002, Lawrence Berkeley National Laboratory, University of California, Berkeley, CA 94270

<sup>‡</sup>Geometrics Inc., 2190 Fortune Dr., San Jose, CA 95131

<sup>§</sup>Department of Materials, Science & Mineral Engineering, University of California at Berkeley, 577 Evans Hall, Berkeley, CA 94270

# 1 Introduction

Both electromagnetic and seismic methods are currently being used for imaging the shallow subsurface. An overview of the use of current seismic reflection imaging methods in the shallow subsurface is given by Steeples et al. (1997). These shallow seismic reflection methods are in effect similar to those used in the petroleum exploration and production industry, but scaled down in size; shotpoint offsets are much reduced, smaller charges or weight-drop sources are used, and geophone spacings as short as 0.5 m (or less) are used to prevent spatial aliasing of Rayleigh waves and air waves. Use of the surface seismic reflection method, based on common-mid-point (CMP) reflection gathers and stacking to image the very shallow subsurface, is often limited by the early record times being dominated by different types of strong and coherent guided wave modes trapped in the weathered layer. Examples of these guided waves are the Rayleigh waves, and the first arrivals refracted at a shallow interface and reflected multiple times by the free surface.

In this paper, we present a method for the imaging of acoustic impedance heterogeneities in the shallow weathered layer by using these strong guided wave modes. We conducted a field experiment involving burial of an empty drum to act as a secondary source of scattered Rayleigh waves and using the first arrival as the illuminating wave. We have processed these data to see if we could detect the presence of the drum.

In an earlier paper (Blonk et al., 1995), we already found that Rayleigh waves can be employed for imaging a large object (a dam) at a distance of 150 m in a tidal flat region, whereas it appeared possible to image scatterers in a carstified near-surface region at distances of more than 1 km. In the present paper, we concentrate on the imaging of small (meter-size) objects at relatively close distances from the receivers (typically less than 10 m) in a region where a significant amount of very shallow near-surface scattering takes place. This somewhat different objective has consequences for the data processing method that are outlined in the present paper.

## 2 Description of the method

We consider scattering of guided waves by shallow subsurface inhomogeneities that are relatively small with respect to the wavelength. The wavefield is generated by a source at surface position  $\mathbf{x}^s$  and is recorded by vertical geophones at surface position  $\mathbf{x}$ . Starting from the frequency-domain form of the elastodynamic wave equation, one can derive a domain-type integral representation for the vertical component of the particle velocity,  $v$ . It is given by

$$v(\omega, \mathbf{x}, \mathbf{x}^s) = v^0(\omega, \mathbf{x}, \mathbf{x}^s) + v^1(\omega, \mathbf{x}, \mathbf{x}^s) , \quad (1)$$

where  $\omega$  denotes the angular frequency, the incident field  $v^0$  is the wavefield that would be present in the absence of scattering objects and the scattered field  $v^1$  accounts for the presence of these objects. In our case, the offset between shot location and nearest receiver is chosen large enough, so that the first arrival is separated in time from the air wave and Rayleigh-wave modes. This first arrival can be a refracted wave, that, after multiple bounces at the free surface, has become a guided wave, propagating mainly in the layer above the refracting interface. We consider the first arrival as the incident field. For shallow objects, the scattered field can be expressed in terms of the scattering impedance  $\xi$  by the relation

$$v^1(\omega, \mathbf{x}, \mathbf{x}^s) = \int_{\text{surface}} dA(\mathbf{x}') \xi(\omega, \mathbf{x}') V^G(\omega, \mathbf{x} - \mathbf{x}') v(\omega, \mathbf{x}', \mathbf{x}^s) , \quad (2)$$

where the Green's function  $V^G$  is the vertical velocity due to an impulsive vertical point-force. In Eq.(2), it is assumed that the near surface, apart from the scattering objects (the “background”), is laterally invariant. The validity of this model has been discussed by Blonk et al. (1995). In principle, shallow scattering objects can now be determined by carrying out the following steps:

1. Separation of the incident wave  $v^0$ , in our case the first arrival, and the scattered wave  $v^1$ . For scattering objects close to the receivers, these can be interfering and

have to be separated by the same type of wavefield separation techniques also used in the processing of VSP and cross-well reflection data.

2. Determination of the Green's function  $V^G$ . Since near-surface scattered waves predominantly consist of Rayleigh waves (Blonk and Herman, 1994), the Rayleigh-wave part is especially important here. In principle, this part can be measured in the field directly by recording the short offsets. In the experiment discussed in the present paper, however, these short offsets were not available and a modeling approach has been used.
3. After determining the scattered field and the Green's function, the impedance function  $\xi$  can be determined in a way similar to seismic migration (see, for instance, Berkhout, 1985), the main difference being that the incident field is the first arrival and the scattered field is a Rayleigh wave. After removing the wave propagation effect from the source to an imaging point  $\mathbf{x}$  and from this imaging point to the receivers, the image of the scattering impedance at location  $\mathbf{x}$  is found at time  $t = 0$ .

The determination of the Green's function at all surface locations to be imaged can be computationally intensive. In section 4, a number of simplifications are discussed, some of which are intimately related to the acquisition geometry used.

### 3 Description of the experiment

The experiment was carried out at the Richmond Field Station of the University of California at Berkeley. The terrain, situated in the Bay margin, can be characterized as a muddy wetland, overgrown with grass and a few small bushes. The upper 30 m of the subsurface consist of tertiary muds; the water table is at 1-2 m depth. The objective was, to investigate to what extent meter-size objects could be detected in the shallow subsurface using the technique of guided-wave imaging. The data-acquisition geometry is shown

in figure 1. The receivers were laid out in a straight line with a spacing of 0.5 m. Both vertical and cross-line horizontal geophones were used. A vertical impact, inline, Betsy gun (8 gauge shells) was used as a source. The experiment using the vertical phones was carried out twice. First, shot records were recorded for six different shot positions spaced 10m apart; the closest shot was situated 40 m from the first receiver. Then, an empty plastic drum having a diameter of about 0.6 m and a length of about 1 m was buried at a distance of 10 m and a depth of 1 m (oriented parallel to the line), after which the experiment was repeated with the same shot locations as before. The objective of this experiment was to compare the strength of the scattered field due to the drum with other near-surface scattering effects. For example, a bush having a diameter of about 1 m was present at a distance of about 3 m from the line. The position of the bush is also shown in figure 1. It was our intention to also perform the same pair of before and after experiments for the cross-line horizontal components, but, due to unforeseen circumstances, we were only able to record the cross-line horizontal data after the drum burial.

## 4 Processing and interpretation of the vertical component data

The processing sequences of the two vertical component data sets (before vs. after drum burial) were identical and consisted of the steps:

*Separation of the incident and scattered waves.*

A shot record, representative of the vertical component data both before and after burial of the drum is shown in figure 2. There was no apparent difference between the before and after shot records to indicate the presence of scattered waves from the drum, thus removal of the dominant first arrival was performed to enhance the presence of the scattered wavefield. Prior to removing the first arrival, receiver statics were determined by picking first-break arrival times and subsequently removed by aligning traces on the

first-break times. Then, the first-arrival wave was subtracted out using a constrained eigenvector wavefield separation technique (Mars and Rector, 1995) leaving behind the scattered Rayleigh waves. Note that any other standard wavefield separation technique could have been used, but we preferred the above method as it resulted in a cleaner separation.

*Determination of the Green's function.*

In principle, the Rayleigh-wave part of the Green's function  $V^G$  can be measured in the field directly by recording the short offsets. In the experiment discussed in the present paper, however, these short offsets were not available and a modeling approach has been used. Since we only imaged at the receiver locations (this is discussed in more detail below), we only needed the Green's function from scattering points at the receiver line to the receivers themselves. Since we were not attempting an accurate true-amplitude imaging, we settled for a Green's function of the form

$$V^G(\omega, x - x') = e^{-j\omega|x-x'|/c_R}, \quad (3)$$

where  $c_R$  is the Rayleigh-wave velocity observed in the data,  $x$  is the receiver coordinate along the line and  $x'$  is the imaging point along the line. This Green's function is kinematically correct for a particular Rayleigh-wave mode but does not account for the proper amplitude behaviour. In order to remedy this somewhat, we have taken the Rayleigh-wave velocity to be complex-valued, i.e.,

$$c_R = |c_R| (1 + j\alpha) \quad (\alpha \geq 0), \quad (4)$$

with  $\alpha = 0.1$ . In this way, the amplitude decay of the Green's function, within the frequency range of interest, was similar to the decay visible in the field data.

*Imaging of the impedance function.*

In order to obtain an image of the scattering impedance function  $\xi$ , wave propagation

effects from the sources and receivers to all surface locations have to be compensated for, followed by an imaging step at time  $t = 0$ . In the frequency domain, this can be achieved by summing the result after wavefield extrapolation over all frequencies (Berkhout, 1985). This type of approach is also taken in Ernst and Herman (1998) for the case of scattered guided waves. For the imaging problem considered here, we are only interested in imaging objects closer than, say, 10 m from the line (which amounts to about 1 wavelength of the dominant frequency of the Rayleigh wave) and a less compute-intensive approach is possible if the velocities do not change too much over this short distance.

As a first step, propagation effects of the guided wave from the source to all points to be imaged have to be removed. For the shots of interest, the path length from the inline sources to a point at position  $(x_1, y_1)$  (with  $y_1$  less than 10 m), differs by less than about 5 percent of the dominant wavelengths from the path length from the source to the receiver at  $(x_1, 0)$ . Hence, we can simply remove propagation effects from the source by correcting for the first-arrival times already determined in the first step of wavefield separation. The total wavefield,  $v$ , after removing propagation effects from the source to the points to be imaged, and adding the results for the different sources, is shown in figure 3 (for the dataset recorded after the burial of the drum).

The removal of the propagation of scattered Rayleigh waves between imaging points and receivers (accounted for by the Green's function  $V^G$  of Eq.(2) can also be simplified. To this aim, we assume all scattering objects to be lumped at the receiver line and discard the integration over the transverse horizontal direction (the  $y$ -direction). After imaging, all objects directly below the line will be imaged at time  $t = 0$ , whereas objects close to the line (at distances not exceeding a wavelength) will be imaged at somewhat later times  $\tau$ , given by

$$\tau = \frac{y}{|c_R|} , \quad (5)$$

where  $y$  is the lateral distance of the object from the receiver line. In this way, objects

directly below the receivers will still be imaged at  $t = 0$ , whereas objects at a few meters distance from the line will be imaged at later times. Since the operator given by Eq(3) is not strictly correct for  $y > 0$ , these objects will not be imaged perfectly, but for lateral distances not exceeding a wavelength, this will be a minor effect.

After wavefield separation of the incident field,  $v_0$ , we obtain the scattered field  $v_1$ ; the result is shown in figure 4. After imaging the scattered field by spatially deconvolving for the Green's function  $V^G$  and performing a temporal deconvolution for the total field  $v$  (see also Eq.(2)), we obtain the impedance function, shown in figure 5, as a function of receiver coordinate and time. At about 53 m, we see the image of the rootsystem of the bush at a travelttime of 8 ms, implying a horizontal distance of 2 m, which is consistent with the surface location of the bush. The width of the image is approximately 1-2 m. There also appears to be another image at a horizontal receiver distance of 35 m. From the image time, we conclude that the crossline distance between the scattering object and the line is about 1.5 m. Since the object has no surface manifestation, we don't know what it is. The size seems to be 1-2 m along the receiver line. *Most important, there appears to be no image of the buried drum.* The dataset that was recorded prior to burying the drum resulted in a image nearly identical to the one shown in figure 5. From this experiment, we therefore conclude that, in this case, we were able to image scattering objects down to sizes of 1-2 meters that are at a maximum distance of 3 m from the receiver line. No objects were imaged at larger distances, indicating that the near-receiver scattering process dominates over all other near-surface scattering processes in this vertical component dataset.

## 5 Interpretation of the crossline horizontal component data

Due to the elliptic polarization of Rayleigh waves, crossline horizontal component geophones should be about as sensitive to crossline scattered Rayleigh waves as the vertical component geophones. But, at the same time, the crossline component is less sensitive to

inline polarized waves, like the illuminating guided wave directly from the source (Blonk and Herman, 1996). The crossline component is also less sensitive to inline, or almost inline, scattered Rayleigh waves originating from heterogeneities close to the line (like the bush at 53 m in our case). Therefore, it should be possible to image objects somewhat further away using the crossline component. One of the crossline horizontal shotrecords after the drum burial is shown in figure 6. In principle, a similar processing sequence would be possible for the horizontal component data as for the vertical component data. But in our experiment, the horizontal component data quality was considerably inferior to the vertical component data, and good first-arrival picks could not be obtained. Therefore, the only processing carried out on the horizontal component data was the killing of bad traces followed by bandpass filtering and  $f - x$  deconvolution to enhance spatial coherency and suppress noise. If three-component geophones had been used, we could have used the vertical component picks and a similar data processing sequence might have been possible as for the vertical component data.

The crossline-horizontal data shown in figure 6 has evidence of a diffraction tail, originating from the bush at 53 m, and of a faint hyperbola, centered at 44 m, with its apex arriving at about 120 ms (i.e., 40 ms after the first arrival). Using the Rayleigh-wave velocity of 240 m/s, this suggests a lateral distance of about 10 m. This hyperbola was also quite consistently visible on the other horizontal records. Unfortunately, we did not record the horizontal data prior to burial of the drum, which implies no definite conclusions can be drawn whether or not this scattering hyperbola is due to the drum or to another heterogeneity. Nevertheless, it seems one can see objects up to a distance of 10m and that the crossline data is indeed more sensitive to crossline scattered Rayleigh waves than the vertical component data is. In the crossline data, the first arrival as well as the (almost) inline scattered waves from the bush and the heterogeneity at 35 m are weaker.

## 6 Conclusions

We have discussed a method for imaging very shallow objects at relatively small distance from the receivers. As an illuminating wave, the first arrival (guided) wave is used. This illuminating wave is converted into scattered Rayleigh waves at shallow heterogeneities. From the field experiment carried out at the Richmond Field Station, we found that we could use the vertical component data to image objects of size 1-2 m at a maximum distance of 3 meters from the receiver line. Objects further away could not be imaged due to the dominant presence of scattered waves from these nearby heterogeneities. Even though the ground appeared well-saturated, there were still deep mud cracks visible at the surface in some places, these being a result of the previous dry summer period.

The crossline horizontal data appear to be more sensitive to crossline scattered Rayleigh waves and less sensitive to the illuminating guided wave and in-line scattered waves. This type of data could therefore enable one to maybe detect objects somewhat further away, but the evidence is lacking to make firm statements based on this experiment. It is, however, consistent with earlier findings (Blonk and Herman, 1996). Probably, the results could be improved by using 3-component geophones and measuring the Green's function by a few separate short-offset experiments with a low-energy source. From other experiments, it was already found that the Rayleigh wave could also be used as the illuminating field (Blonk et al, 1995) and that a dam could be imaged at a distance of 150 m, whereas for another dataset, objects could be imaged at distances of more than 1 km. The possibility of detecting shallow objects is therefore very dependent upon the size of the object, their contrast, and the properties of the shallow subsurface, but there are definitely interesting possibilities to be investigated.

## Acknowledgments

This research has been carried out while Gérard Herman was a Phoebe Apperson Hearst visiting professor in the Department of Materials Science and Mineral Engineering with the financial support of the University of California at Berkeley and the Dutch Technology Foundation. This support is gratefully acknowledged. The Richmond Field data was obtained with the help of John Washbourne, Qicheng Dong and Tao Zhen of the Engineering Geoscience Group at the Lawrence Berkeley National Laboratory. Their assistance was invaluable in this “Dutch day in the field” with a lot of rain and mud. The equipment used during the experiment was made available by Geometrics Inc.

## References

- Berkhout, A.J., 1985, Imaging of acoustic energy by wavefield extrapolation (3rd edition): Elsevier.
- Blonk, B., and Herman, G.C., 1994, Inverse scattering of surface waves: A new look at surface consistency: *Geophysics*, **59**, 963-972.
- Blonk, B., Herman, G.C., and Drijkoningen, G.G., 1995, An elastodynamic inverse scattering method for removing scattered surface waves from field data: *Geophysics*, **60**, 1897-1905.
- Blonk, B., and Herman, G.C., 1996, Removal of scattered surface waves using multicomponent seismic data: *Geophysics*, **61**, 1483-1488.
- Ernst, F.E., and Herman, G.C., 1998, Removal of scattered guided waves from seismic data in laterally varying media: accepted for publication in *Wave Motion*.
- Mars, J.I., and Rector, J.W., 1995, Constrained eigenvectors: A means to separate aliased arrivals: 65th Ann. Internat. Mtg., Soc. Expl. Geophys., Expanded Abstracts, 49-

52.

Steeple, D.W., Green, A.G., McEvilly, T.V., Miller, R.D., Doll, W.E., and Rector, J.W.,  
1997, A workshop examination of shallow seismic reflection surveying: The Leading  
Edge, **16**, 1641-1647.

## Figure Captions

1. Plan view of the Richmond Field Station experiment. The objective was, to investigate to what extent meter-size objects could be detected in the shallow subsurface using the technique of guided-wave imaging. The receivers were laid out in a straight line with a spacing of 0.5 m. Both vertical and cross-line horizontal geophones were used. The experiment using the vertical phones was carried out twice: both before and after burial of an empty plastic drum having a diameter of about 0.6 m and a height of about 1 m. Shot records were recorded for six different shot positions spaced 10m apart; the closest shot was situated at 40 m from the first receiver. The crossline horizontal data were only recorded after burial of the drum.
2. A shot record, representative of the vertical component datasets.
3. The total wavefield,  $v$ , for the dataset recorded after the burial of the drum. The effect of propagation of the guided wave from each shot to the region close to the receiver line has been removed by aligning the traces on their first-break times, after which the shots have been stacked.
4. The scattered field,  $v_1$ , obtained after wavefield separation of the incident field from the scattered field. The dominant Rayleigh-wave velocity appears to be  $c_R = 240$  m/s (note that the traces are still aligned on the first-break picks).
5. After imaging the scattered field as a function of receiver coordinate and time  $t$ , we obtain the impedance function shown here. At about 53 m, we see the image of the rootsystem of the bush at a travelttime of about 8 ms, implying a horizontal distance of about 2 m, which is consistent with the surface location of the bush. The width of the image is about 1-2 m. There also appears to be another image at a horizontal receiver distance of about 35 m. From the image time, we conclude that the crossline distance between the scattering object and the line is about 1.5 m. Since the object

has no surface manifestation, it is unknown what it is. The size seems to be 1-2 m along the receiver line. There appears to be no image of the buried drum from the vertical component of the data.

6. A typical 48-channel recording of the crossline horizontal component after the drum burial. Apart from a diffraction tail originating from the bush at 53 m, we see a faint hyperbola centered at 44 m, with its apex arriving at 120 ms, which is 40 ms after the first arrival. Using a Rayleigh-wave velocity of 240 m/s, this suggests a lateral distance of about 10 m. This hyperbola was also quite consistently visible on the other horizontal records. It seems one can see objects up to a distance of 10 m, and that the crossline data is more sensitive to crossline scattered Rayleigh waves than the vertical component data is. In the crossline data, the first arrival as well as the (almost) inline scattered waves from the bush and the heterogeneity at 35 m are weaker. The first arrival occurs at about 80 ms, the airwave starts at about 180 ms, and the low-frequency groundroll (Rayleigh wave) starts at about 270 ms.

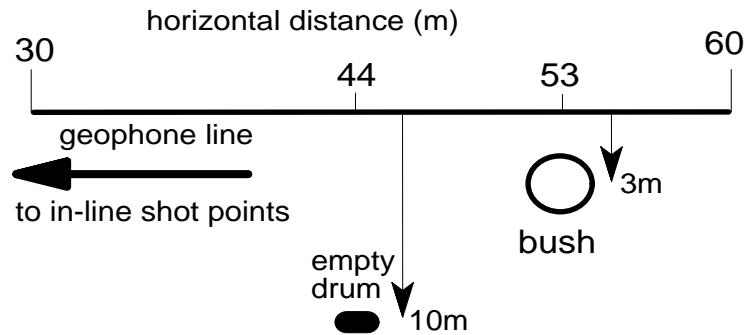


Figure 1: Plan view of the Richmond Field Station experiment. The objective was, to investigate to what extent meter-size objects could be detected in the shallow subsurface using the technique of guided-wave imaging. The receivers were laid out in a straight line with a spacing of 0.5 m. Both vertical and cross-line horizontal geophones were used. The experiment using the vertical phones was carried out twice: both before and after burial of an empty plastic drum having a diameter of about 0.6 m and a height of about 1 m. Shot records were recorded for six different shot positions spaced 10 m apart; the closest shot was situated at 40 m from the first receiver. The crossline horizontal data were only recorded after burial of the drum.

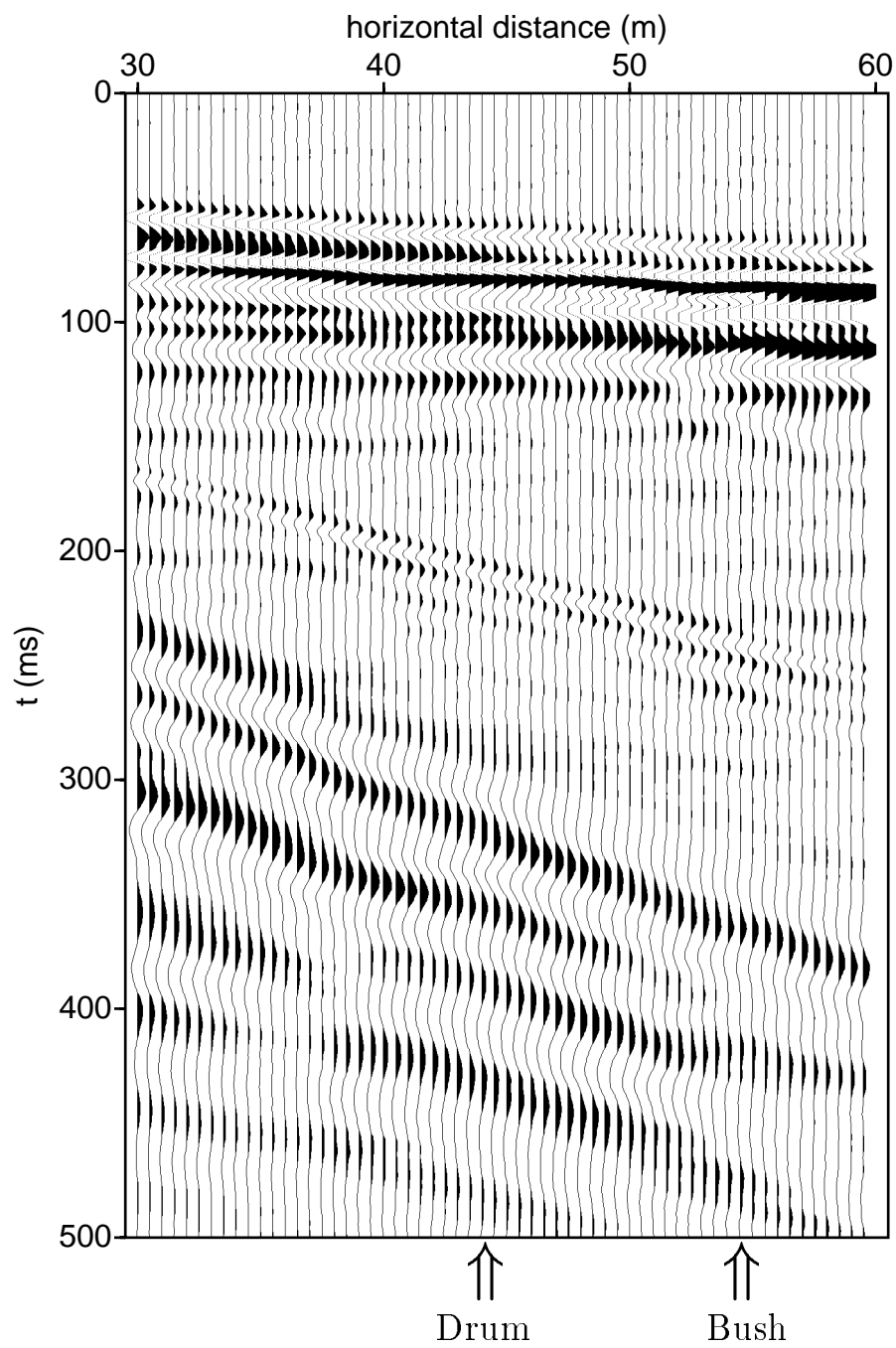


Figure 2: A shot record, representative of the vertical component datasets.

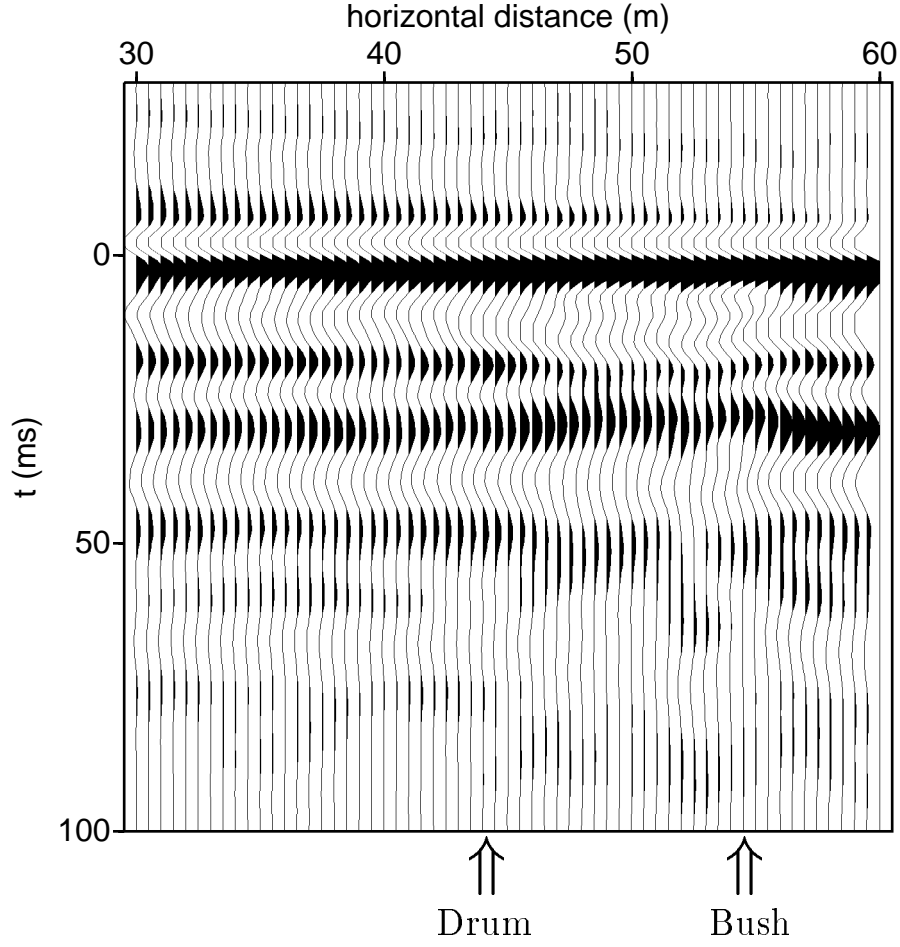


Figure 3: The total wavefield,  $v$ , for the dataset recorded after the burial of the drum. The effect of propagation of the guided wave from each shot to the region close to the receiver line has been removed by aligning the traces on their first-break times, after which the shots have been stacked.

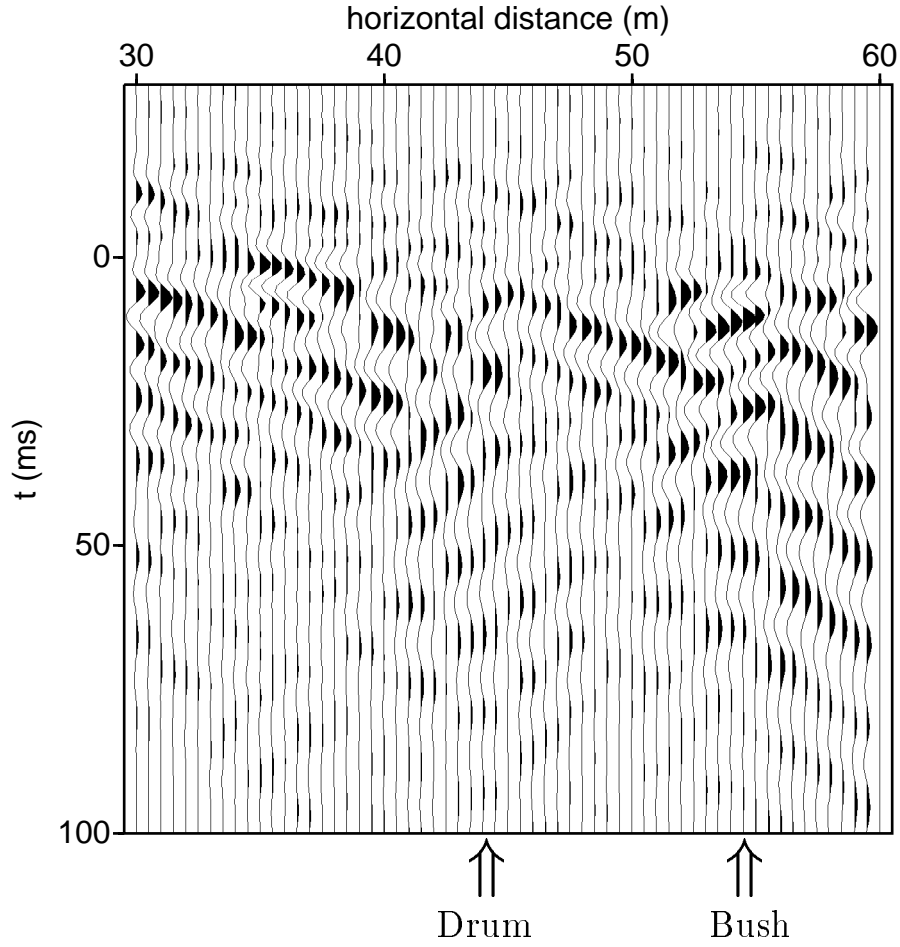


Figure 4: The scattered field,  $v_1$ , obtained after wavefield separation of the incident field from the scattered field. The dominant Rayleigh-wave velocity appears to be  $c_R = 240$  m/s (note that the traces are still aligned on the first-break picks).

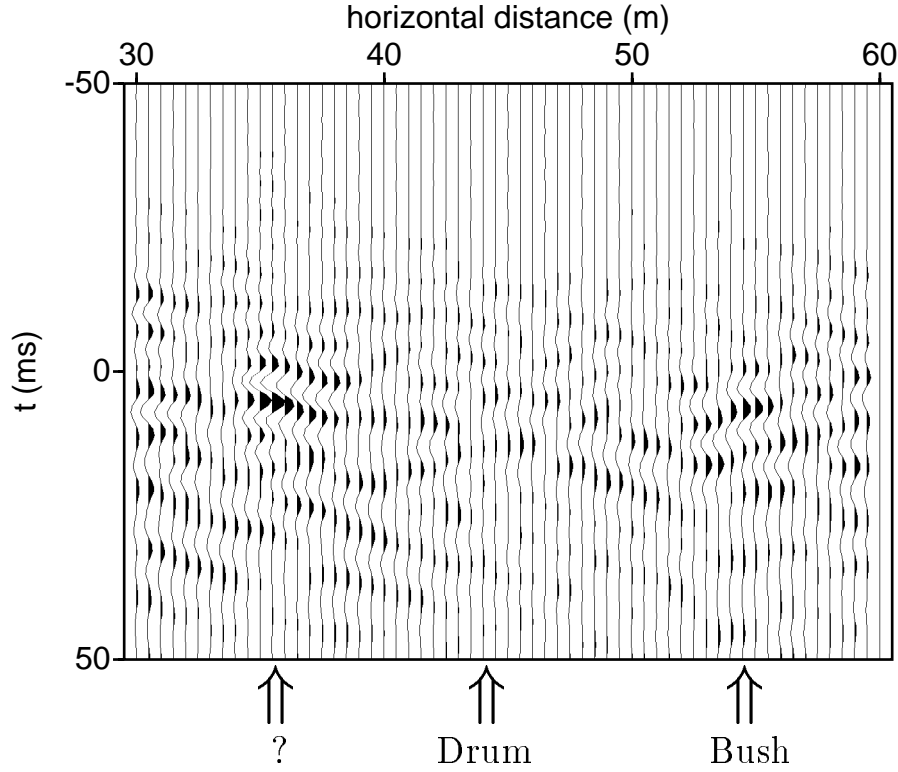


Figure 5: After imaging the scattered field as a function of receiver coordinate and time  $t$ , we obtain the impedance function shown here. At about 53 m, we see the image of the rootsystem of the bush at a traveltime of about 8 ms, implying a horizontal distance of about 2 m, which is consistent with the surface location of the bush. The width of the image is about 1-2 m. There also appears to be another image at a horizontal receiver distance of about 35 m. From the image time, we conclude that the crossline distance between the scattering object and the line is about 1.5 m. Since the object has no surface manifestation, it is unknown what it is. The size seems to be 1-2 m along the receiver line. There appears to be no image of the buried drum from the vertical component of the data.

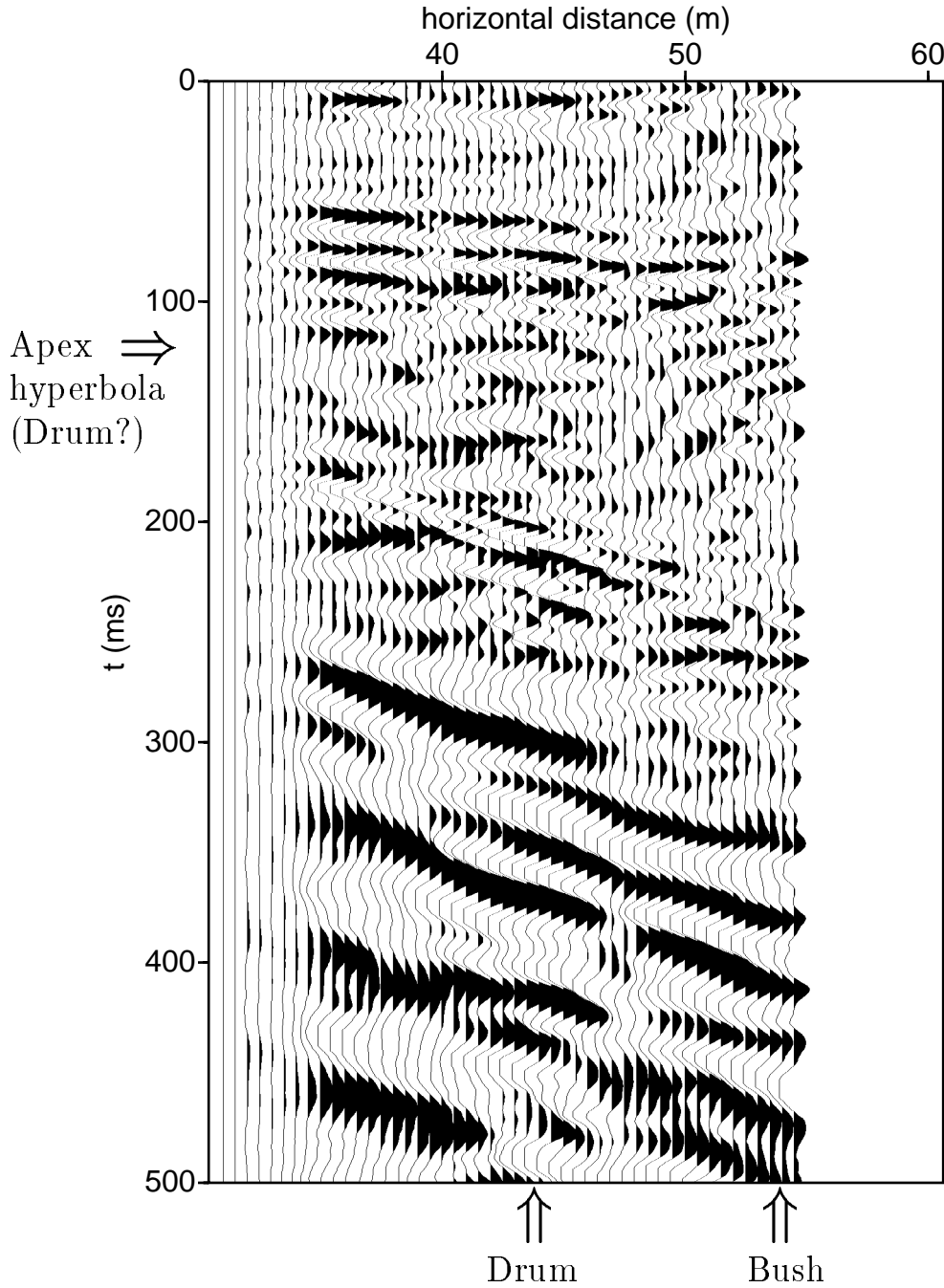


Figure 6: A typical 48-channel recording of the crossline horizontal component after the drum burial. Apart from a diffraction tail originating from the bush at 53 m, we see a faint hyperbola centered at 44 m, with its apex arriving at 120 ms, which is 40 ms after the first arrival. Using a Rayleigh-wave velocity of 240 m/s, this suggests a lateral distance of about 10 m. This hyperbola was also quite consistently visible on the other horizontal records. It seems one can see objects up to a distance of 10 m, and that the crossline data is more sensitive to crossline scattered Rayleigh waves than the vertical component data is. In the crossline data, the first arrival as well as the (almost) inline scattered waves from the bush and the heterogeneity at 35 m are weaker. The first arrival occurs at about 80 ms, the airwave starts at about 180 ms, and the low-frequency groundroll (Rayleigh wave) starts at about 270 ms.